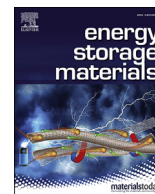




Contents lists available at ScienceDirect

Energy Storage Materials

journal homepage: www.elsevier.com/locate/ensm

Thermally stable, nano-porous and eco-friendly sodium alginate/attapulgite separator for lithium-ion batteries

Qingquan Song^{a,1}, Aijun Li^{a,b,1}, Lei Shi^{c,1}, Cheng Qian^a, Tony Gordon Feric^d, Yanke Fu^a, Hanrui Zhang^a, Zeyuan Li^a, Peiyu Wang^a, Zheng Li^e, Haowei Zhai^a, Xue Wang^a, Martin Dontigny^f, Karim Zaghib^f, Ah-Hyung (Alissa) Park^d, Kristin Myers^c, Xiuyun Chuan^b, Yuan Yang^{a,*}

^a Program of Materials Science and Engineering, Department of Applied Physics and Applied Mathematics, Columbia University, New York, NY, 10027, United States

^b Key Laboratory of Orogenic Belts and Crustal Evolution, School of Earth and Space Sciences, Peking University, Beijing, 100871, China

^c Department of Mechanical Engineering, Columbia University, New York, NY, 10027, United States

^d Department of Chemical Engineering, Columbia University, New York, NY, 10027, United States

^e Jiangsu Qingtao Energy S&T Co., Ltd, Huai-an, 211700, China

^f IREQ—Institute Recherche D'Hydro-Québec 1800 Boulevard Lionel Boulet, Varennes, Québec, J3X 1S1, Canada

ARTICLE INFO

Keywords:

Sodium alginate

Attapulgite

Separator

Lithium-ion batteries

ABSTRACT

Traditional polyolefin separators are widely used in lithium-ion batteries. However, they are subject to thermal shrinkage which may lead to failure at elevated temperatures, ascribed intrinsically to their low melting point. And besides, recycling of spent lithium-ion batteries mainly focuses on precious metals, like cobalt, while other components such as separators are usually burnt or buried underground, causing severe hazards for the local environment, such as “white pollution”. Therefore, to solve the aforementioned problems, we incorporated attapulgite (ATP) nanofibers, a natural mineral, into sodium alginate (SA), a biodegradable polysaccharide extracted from brown algae, through a phase inversion process, whereby a porous separator was prepared. The resulting SA/ATP separator is endowed with high thermal and chemical stability, enhanced retardancy to fire, and excellent wettability with commercial liquid electrolyte (420% uptake). Attractive cycling stability (82% capacity retention after 700 cycles) and rate capability (115 mAh g⁻¹ at 5 C) in LiFePO₄/Li cells are achieved with such separator, additionally. Moreover, as both ingredients are nontoxic, this eco-friendly separator can degrade in soil without inducing any contamination. This work offers a viable choice to process a thermally stable, eco-friendly separator and open up new possibilities to improve the safety of batteries while alleviating the “white pollution”.

1. Introduction

Lithium-ion batteries (LIBs) have found wide applications in portable electronics and electric vehicles which have gained rapidly growing popularization over past few years, due to their high energy density, long cycle life and decreasing cost [1–4]. A battery consists of cathode and anode which are isolated from each other by a porous polymer film, or separator. The separator plays a key role as it is placed between the cathode and anode to prevent their physical contact, while enabling free movement of ions and isolating the electronic flow.

The separators widely used are made of polyolefins, a class of polymers produced from an olefin like ethylene or propylene as the monomer,

which usually feature low melting point [5]. Therefore, the polyolefin separators suffer from large thermal shrinkage at temperatures beyond their melting point, which is owing to their inadequate thermal stability and may cause severe safety issues when short circuit occurs due to lithium plating [6]. Typically, ceramic coatings, such as Al₂O₃ and SiO₂, are extensively used to enhance thermal stability of separators [7,8]. However, the coating layers always tend to block some pores of the polymer host, reducing the utility of the coating [9]. Moreover, a fact often under deep disguise is that, when a battery hits its retirement age, mainly the cathode material will be recycled, as the precious metals like cobalt in it is of most economic values; while in contrast, the separator is usually burned or buried under ground [10]. The annual consumption of

* Corresponding author.

E-mail address: yy2664@columbia.edu (Y. Yang).

¹ Q. Q. Song, A. J. Li and L. Shi contributed equally to this paper.

<https://doi.org/10.1016/j.ensm.2019.06.033>

Received 23 March 2019; Received in revised form 24 June 2019; Accepted 26 June 2019

Available online xxx

2405-8297/© 2019 Elsevier B.V. All rights reserved.

polyolefin separators for lithium-ion batteries in the world is estimated to have reached 2 billion square meters, weighing around 40 thousand tons (the process of calculation is in supporting information). Those waste polyolefin separators with stable chemical structure and thereby high resistance to natural degradation [11] then aggravate the plastic pollution, also known as the “white pollution”, which has been a formidable threat to the sustainable development of human society. Hence in order to solve those aforementioned problems, it is considered demanded to fabricate a separator with high thermal stability at elevated temperatures based on natural and/or degradable materials.

The increasing concerns on the plastic pollution have given birth to a shift towards biodegradable materials [12], which has brought the polysaccharide under the spotlight as a promising and eco-friendly biomaterial [13]. As a major constituent widely existing in the brown algae, sodium alginate (SA) has been widely used in food industry, and tissue engineering as scaffold materials, due to its biodegradability, biocompatibility and sustainability [14–17]. Encouragingly, it has also found some applications in lithium ion batteries, such as binders, especially for anode materials with large volume expansion [18]. SA is attractive as its strength suffers little deterioration and it is immune to swelling when soaked in organic electrolytes [19–21]. SA separators prepared upon electrospinning have been reported as well, where the resulting material shows good electrochemical performance, high chemical stability and extremely high porosity, while exhibiting decent mechanical strength [22]. However, a drawback of the membranes prepared upon electrospinning is their large pore sizes that can be a few tens of micrometers, as the large pores tend to become free path for the diffusion of cathode particles to anode, thereby resulting in local short circuit [23]. Moreover, an inorganic additive is also required in necessity to endow the composite membrane with high thermal stability and fire retardancy. Once used as additive to enhance the toughness and mechanical strength of polymer [24], attapulgite (ATP), a type of common and abundant clay mineral, then came into our view. ATP is a magnesium aluminum phyllosilicate with formula $(\text{Mg, Al})_2\text{Si}_4\text{O}_{10}(\text{OH})\cdot 4(\text{H}_2\text{O})$ and many desirable properties. In the first place, ATP possesses an excellent thermal stability, as it can maintain its structure even at temperature of 800 °C [25]. Furthermore, ascribed to its fibrous hollow morphology, ATP itself has remarkably high surface area and has been utilized to adsorb organics on the clay surface [26], which is considered to enhance electrolyte absorption of the resulting material. It is also commonly found that ceramic additives can absorb HF generated during cycling and thereby enables longer cycle life of the cells [27]. Last but not least, ceramic additives can help enhance electrolyte wettability to enable fast and bubble-free filling of electrolyte. Therefore, in this study, we synthesized the composite separator composed of SA as the substrate and ATP nanofiber as the additive through a phase inversion process. The resulting separator is found to possess high thermal stability and fire retardancy, excellent wettability with liquid electrolyte (420% uptake). Meanwhile, such SA/ATP separator endows $\text{LiFePO}_4/\text{Li}$ cells with attractive cycling stability (82% capacity retention after 700 cycles) and rate capability (115 mAh g^{-1} at 5 C). This work provides a viable option to process a thermally stable, degradable separator, and enlightens new avenue to improve the safety of LIBs and alleviate the “white pollution”.

2. Experimental section

2.1. Materials

The sodium alginate was purchased from Sigma Aldrich (St. Louis, MO). The attapulgite nanofibers were purchased from Guangming ATP Co. Ltd (Anhui, China). The ATP nanofibers were baked in a furnace at 200 °C for 6 h to remove bond water before use.

2.2. Material characterization

Crystal structures of ATP, SA and SA/ATP membranes were analyzed

by a PANalytical XPert3 Powder XRD with Cu K α radiation run at 45 mA and 40 V. Morphology of samples was characterized on SIGMA VP Zeiss scanning electron microscopy (SEM) with an energy dispersive spectrometer. The detailed morphology of ATP fibers were executed with FEI TALOS F200X transmission electron microscopy (TEM). The ATP powder for TEM analysis was prepared by drop-casting ATP ethanol dispersion onto a TEM grid. The N₂ adsorption–desorption isotherms were measured on a Micromeritics ASAP 2020 HV system at 77 K. The specific surface area of sample was calculated using the multiple-point Brunauer–Emmett–Teller (BET) method. Pore size distribution was determined using Barrett–Joyner–Halenda (BJH) method. Fourier-transform infrared spectroscopy (FT-IR) of the separator before and after being heated was performed with a Nicolet 6700 spectrometer (Thermo Fisher Scientific Inc.) equipped with a Czteck SurveyIR Diamond Attenuated Total Reflectance (ATR) cell. Reflection mode was employed with the aperture set to 2000 μm . The spectra were obtained under ambient conditions with resolution of 8 cm^{-1} in the wavenumber range of 400–2000 cm^{-1} . The sample collection time was 2.5 min. Thermal gravimetric analysis (TGA) of the samples was carried out with a TA Instruments Q500. The temperature-rising speed is 10 °C min^{-1} over the entire temperature range from 25 to 800 °C in air. The porosity was determined by the weight difference of the samples before and after being soaked in methyl silicone oil according to the equation as follows:

$$P = \frac{W_2 - W_1}{\rho V} \times 100\%$$

where P is the porosity, W_2 and W_1 are the wet weight and dry weight of the samples, ρ is the density of methyl silicone oil (0.96 g cm^{-3}), and V is the apparent volume of samples. The theoretical porosity of the samples based on their real mass and volume, and density of ATP (2.4 g cm^{-3}) and SA (1.65 g cm^{-3}) was also calculated.

2.3. Thermal stability test

A piece of SA/ATP 1–4 membrane and a piece of Celgard 2325 PE separator were heated at 250 °C in a furnace for 2 h. Once after being heated, the samples were taken out and observed. To test the fire retardancy, both SA/ATP membranes and Celgard 2325 were hung over the flame of a lighter to observe their combustion behavior.

2.4. Electrolyte wettability test

The Celgard 2325 separator and SA/ATP membranes were hung over the electrolyte with one end immersed in it. The immersion-height was then compared after 10 min. In the meanwhile, the electrolyte uptake was also measured to provide more supporting evidence. In that case, the SA/ATP membranes and the Celgard 2325 were immersed in commercial electrolyte for 2 h and then taken out to measure the electrolyte uptake after wiping away the electrolyte superficially absorbed on the surface of the membrane. The value of electrolyte uptake (E) by the separator was determined by using the following equation:

$$E = \frac{W_2 - W_1}{W_1} \times 100\%$$

where W_2 and W_1 are the wet weight and dry weight of the samples.

2.5. Electrochemical test

The conductivity of Celgard 2325 and SA/ATP membranes with different composition in liquid electrolyte (1 M LiPF_6 in EC/DEC, (EC: DEC = 1:1, w/w)) was measured by using cells assembled in the layout of stainless steel/separator/stainless steel. Electrochemical impedance spectroscopy (EIS) measurements were carried out over the frequency range from 10⁶ to 0.1 Hz with 10 mV amplitude. The temperature-dependent ionic conductivity of the SA/ATP separator was measured at

temperature ranging from 30 °C to 80 °C with an interval of 10 °C, and was plotted to calculate the activation energy based on the Arrhenius equation

$$\sigma = A \exp\left(\frac{-E_a}{RT}\right)$$

where σ is the ionic conductivity, A is the pre-exponential factor, E_a is the activation energy, T is temperature, and R is the ideal gas constant. Linear sweep voltammetry (LSV) of the samples was conducted with a sweep rate of 0.1 mV s⁻¹ between 2.5 and 5.0 V, upon using a stainless-steel electrode as the working electrode and lithium as the reference electrode. Li/Li symmetric cell cycling was conducted under the current density and capacity of 1 mA cm⁻² and 1 mAh cm⁻², respectively. For the LFP/Li cell test, LFP cathode was prepared using the doctor-blade casting of electrode slurry. A slurry that contained LFP (80 wt%), carbon black (10 wt%), and poly(vinylidene fluoride) (10 wt%) were dissolved in N-methyl-2-pyrrolidone was cast onto an aluminum foil. The cast film was dried in air at 110 °C for 12 h. The mass loading of active material in cathode was fixed at 4.5 mg cm⁻². A LAND battery testing system was used to conduct the long cycling test at charge/discharge rate of 0.5 C and 1 C (1 C = 170 mA g⁻¹), respectively. The charge and discharge cut-off voltage of the cell was set between 2.5 and 3.8 V.

2.6. Tensile test

Tensile tests were performed on a universal testing machine (Micro-tester 5948, Instron Inc., Norwood, MA) equipped with the grips attached to the 50 N load cell (Instron Inc., Norwood, MA, 0.25% accuracy of indicated load). Before each test, the load cell was balanced sufficiently, and each sample was aligned vertically to make sure the sample was in the uni-axial tension state. During the tension tests, the strain rate was kept as 0.2% per second to guarantee the quasi-static state of the whole process to avoid the dynamical and viscoelastic effects. The stress (σ) and strain (ϵ) of the sample during the test was calculated using following equations. The Young's modulus of the sample was obtained using the quotient of the stress over the strain.

$$\sigma = \frac{F}{wt}$$

$$\epsilon = \frac{d}{l}$$

Where σ is the stress, ϵ is the strain, F is the force response recorded by Instron, w is the width, t is the thickness, d is the extension of the length, l is the original length, of the sample. Significant changes in the width and

thickness of the sample were not observed, and therefore the cross-sectional area was treated as constant.

3. Results and discussion

The phase inversion process was applied to prepare the porous membranes, the mechanism and overall procedure of which are described in Fig. 1. In brief, as illustrated in Fig. 1a, the polymer ingredient is dissolved in a mixture of water (solvent) and NMP (non-solvent), where NMP has a boiling point of 202 °C, much higher than that of water (100 °C), followed by the application of the solution. After both solvent and non-solvent evaporate in sequence, a porous membrane is formed [28,29]. As demonstrated in Fig. 1b, SA powder and ATP nanofibers with different weight ratios (SA: ATP = 1:1, 1:2, 1:3 and 1:4, w/w, respectively) were blended in the mixture of DI water and NMP (DI water: NMP: SA = 50:1:1, w/w/w), under continuous stirring and heating at 80 °C for 6 h. The solution then underwent a 3-h ultrasonic treatment. After a homogeneous solution was formed, it was cast on a piece of glass by using a doctor blade (casting speed = 2 cm s⁻¹). The as-cast solution was then dried at ambient conditions till both water and NMP evaporated. The resulting membrane was then peeled off from the glass and dried in a vacuum oven at 105 °C for 6 h. The thickness of the material thus prepared is measured to be ~20 μ m by using a micrometer. According to the weight ratio of SA to ATP, the prepared membranes are denoted as SA/ATP 1-X (X = 1, 2, 3, 4) hereby.

The microstructure of ATP nanofibers was first characterized by transmission electron microscopy (TEM). Through the TEM image (Fig. 2a), it is observed that the ATP nanofibers are roughly 1 μ m in length with a diameter of ~50 nm. And the diffraction pattern shows a polycrystalline structure, where the rings match with (-121) and (-161) planes in attapulgite (JCPDS No. 21-0958). The results of BET analysis show that the ATP nanofiber has the feature of mesoporous absorbents that is told from its IV-type adsorption and desorption isotherm (Fig. S1), and possesses a hollow tunnel structure, where most pores are of sizes within 10 nm (Fig. 2b). The homogeneity is of great significance for the performance of a separator, and it requires the composition and microstructure to be as uniform as possible throughout the material, which is regarded conducive to suppressing the growth of dendritic lithium via enabling uniform lithium flux [30]. Also, pore size less than 1 μ m is required, as the nano-porous structure is considered able to prevent cathode particles from penetrating the separator [31]. The optical image of the resulting membrane (Fig. 2c) is uniformly pale yellow-colored across its surface, suggesting its high homogeneity. Indeed, with the existence of ATP nanofibers proved by X-ray diffraction (XRD) (Fig. S2), where sharp characteristic peaks of ATP can be observed, the scanning electron microscopy (SEM) images (Fig. 2d) show that the SA/ATP

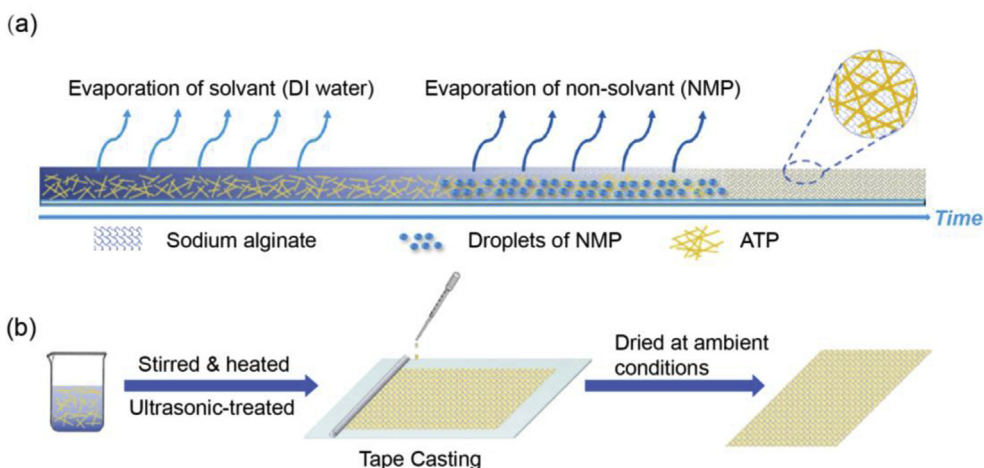


Fig. 1. Schematic illustration of (a) the mechanism of phase inversion method and (b) the overall procedure of the material preparation.

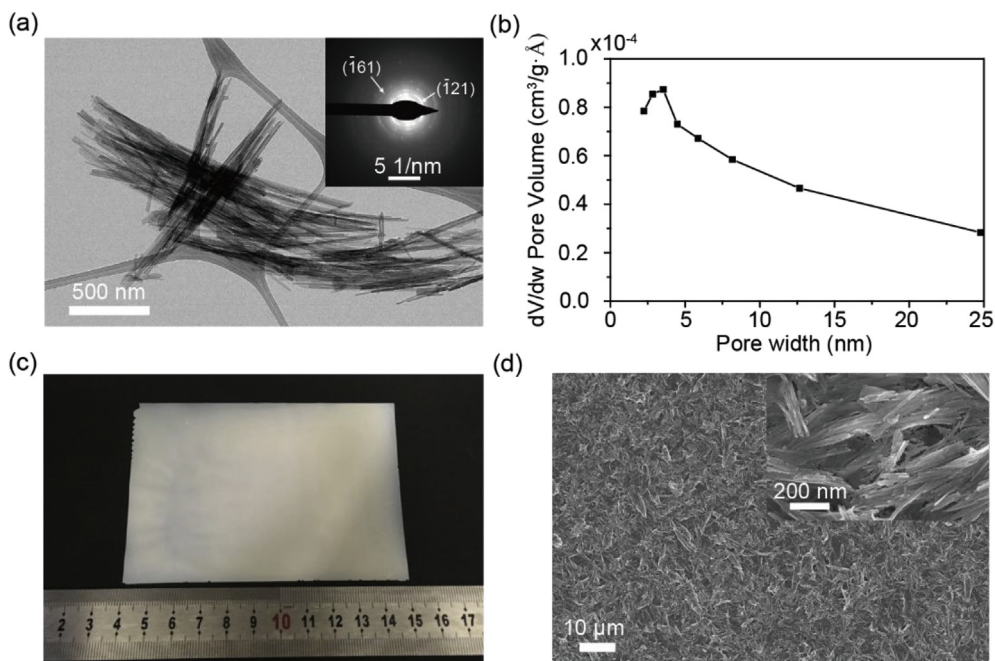


Fig. 2. Characterization of the ATP nanofibers and SA/ATP 1–4 membrane. (a) The TEM image of ATP fibers. The inset image is the diffraction pattern of ATP. (b) Pore size distribution of ATP nanofibers. (c) An optical image and (d) an SEM image of the SA/ATP 1–4 membrane.

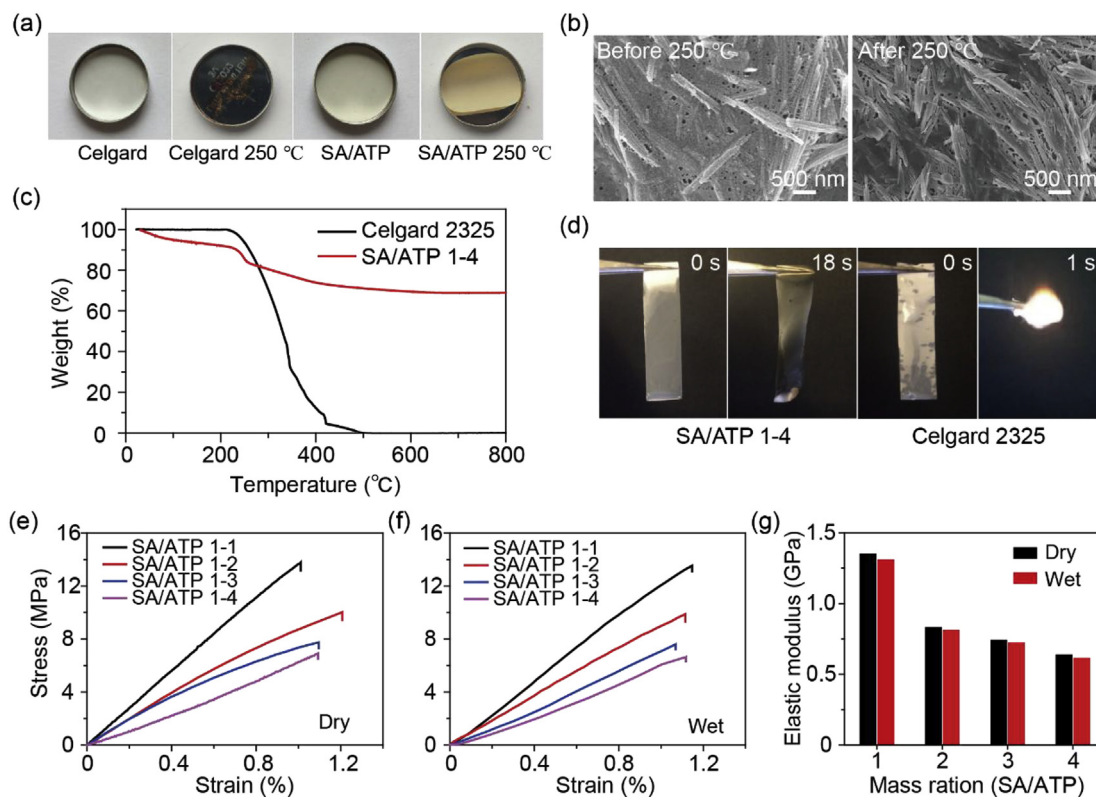


Fig. 3. Thermal stability and mechanical strength of Celgard 2325 and SA/ATP 1–4 separators. (a) Optical images of Celgard 2325 and SA/ATP 1–4 separators before and after being heated in a furnace at 250 °C for 2 h. (b) SEM images of SA/ATP 1–4 separator before (left) and after (right) the test in (a). (c) TGA curves of Celgard 2325 and SA/ATP 1–4 separators. (d) Combustion test of Celgard 2325 and SA/ATP 1–4 separators wetted with commercial carbonate electrolyte (1 M LiPF₆ in EC/DEC, (EC: DEC = 1:1, w/w)). (e) Dry and (f) wet stress-strain curves of SA/ATP separators with different compositions, and (g) comparison of corresponding Young's modulus of the separators.

membranes possess homogeneous morphology where the ATP fibers and nano-sized pores are evenly distributed, which can be further proved by energy dispersive spectroscopy (EDS) images (Fig. S3), in which silicon

and aluminum, two characteristic elements of ATP, are uniformly dispersed. In Fig. S4, it is observed that the increasing addition of ATP does not interfere the distribution of ATP nanofibers and pores

throughout the membrane.

High thermal stability is an essential requirement for separators which enables them to maintain their dimension in case of elevated temperatures due to short circuit caused by overcharging [32]. As shown in Fig. 3a, after being heated in a furnace at 250 °C for 2 h, the Celgard 2325 separator had already burned away. While in comparison, the SA/ATP membrane still remained intact. SEM was then used to observe the change in its microstructure. Through the SEM images, it is found that the nano-porous structure of SA/ATP 1-4 separator was retained (Fig. 3b). As the Celgard separator burnt away after the test, another piece of sample was heated at 250 °C for 5 min; however, even after such a short period, the pores of Celgard separator completely disappeared (Fig. S5). And through the measurement of its diameter and thickness before and after the test, it is found that the SA/ATP sample suffered a tiny thermal shrinkage less than 1%. XRD and FT-IR spectra of the SA/ATP 1-4 separator before and after being heated were also provided. As shown in Fig. S6a, it is noticed that the characteristic peaks in the XRD pattern of SA/ATP 1-4 separator remained. Those intensified peaks of heated SA/ATP 1-4 come from ATP. As for FT-IR (Fig. S6b), after being heated, there is almost no change in the spectrum of SA/ATP 1-4 separator. The absorption bands around 1617 cm^{-1} and 1414 cm^{-1} are attributed to stretching vibrations of asymmetric and symmetric bands of carboxylate anions, respectively [33]. The bands at 421 cm^{-1} and 978 cm^{-1} are assigned to the bending vibration of Si-O-Si bonds and stretching vibration of Si-O bonds, respectively [34].

Moreover, a home-made ATP-coated PE separator, a commercial LLTO-coated PE separator and a commercial Al_2O_3 -coated PE separator were heated at 250 °C for 5 min and then compared as well to make prominent the utility of ATP in enhancing thermal stability of the separators. All three ceramic-coated separators are composed of a coating layer with thickness of around 4 μm and a 12- μm thick PE substrate, and their total thickness is similar to that of the SA/ATP separators. The optical images (Fig. S7) tell that after being heated, both LLTO-coated PE separator Al_2O_3 -coated PE separator severely curled up and shrank, while the ATP-coated one was still able to maintain its dimension to a significant extent due to the thermally and mechanically stable ATP network. The SEM images were also taken to observe the change in their microstructure. As shown in Figs. S8 and S9, for the LLTO-coated and the Al_2O_3 -coated ones, after being heated, their coated side markedly wrinkled; while on their bare side, the pores completely disappeared, meaning they have lost their function as a battery separator. The distinct contrast demonstrates the effectiveness of ATP nanofiber network to provide mechanical strength, which also leads to excellent thermal stability of SA/ATP observed in Fig. 3a. Finally, the curves of thermal gravimetric analysis (TGA) of the SA/ATP 1-4 membrane also shows that it can withstand high temperatures up to 800 °C (Fig. 3c), which is also true for SA/ATP membranes with other compositions (Fig. S10).

When a short circuit does occur, the battery may catch on fire if the temperature dramatically rises above the flash point of the electrolyte [35]. Therefore, a separator with retardancy to fire can ensure safety to a considerable degree. As shown in Fig. 3d, it is observed that the Celgard 2325 separator immediately shrank once touching the flame of the lighter and was completely burnt away very quickly. While in comparison, when wetted by liquid carbonate electrolyte, even though the SA in the SA/ATP separator was also more or less burnt away when it touched the flame, the ATP fibers were still able to maintain the dimension of the membrane to a remarkable extent and assured that the membrane did not catch on fire at all. The result of the flame test confirms that ATP fibers indeed endow the material with retardancy to combustion as well as the ability to maintain its dimension at pronouncedly high temperature. And through comparison of combustion behavior of SA/ATP membranes with different compositions (Figs. S11 and S12), a trend is found that, the higher the ATP content, the better fire retardancy is obtained, be the membranes wetted with liquid electrolyte or not.

In addition to high thermal stability, the separator is also required to possess adequate mechanical strength to suffice for cell assembly and,

meanwhile, be able to maintain its mechanical strength when immersed in liquid electrolyte [36]. From the stress strain curves (Fig. 3e and f), it is shown that descending ATP content increases the maximum stresses the SA/ATP membranes can withstand, from around 6 MPa for SA/ATP 1-4 to 14 MPa for SA/ATP 1-1. Moreover, the electrolyte actually causes little deterioration to the mechanical strength of the composite membranes, where there is only tiny change in their fracture stresses and Young's modulus (Fig. 3g and Table S1), as the SA is immune to swelling in liquid electrolyte, which further proving their qualification to be used as separators in lithium-ion batteries.

With high thermal stability and adequate mechanical strength as two prerequisites, a qualified separator should also be compatible with the liquid electrolyte so that it can rapidly get wetted [37]. From the results of electrolyte uptake (Fig. 4a), it is found that all SA/ATP membranes have better electrolyte uptake capacity than Celgard 2325. After being immersed in electrolyte for 2 h, the electrolyte uptake of Celgard 2325 is slightly more than 130%, which is similar to previous report [38]. While, obviously, SA/ATP 1-4 stands out with the highest uptake, 420% versus 342%, 265%, and 240% for SA/ATP 1-3, SA/ATP 1-2, and SA/ATP 1-1, respectively. The result matches the specific surface area measured upon BET analysis (Fig. S13), where all SA/ATP membranes are found to possess much higher specific surface area than Celgard separator, among which the SA/ATP 1-4 membrane steps forward out of its peers with the highest value (163.35 $\text{m}^2 \text{g}^{-1}$), around 6 times as high as that of its Celgard counterpart (26.63 $\text{m}^2 \text{g}^{-1}$). However, it is interesting to notice that the result of electrolyte uptake is against the indication from the porosity measurement, where the SA/ATP 1-4 membrane with the highest content of ATP and showing the best compatibility with liquid electrolyte has the lowest porosity, unexpectedly. The reason is suspected to be that, a considerable portion of the pores are actually "inactive" that are not interconnected, and the SA/ATP membranes may rely more on the networked ATP nanofibers to absorb electrolyte. If the amount of ATP is small, like the case of SA/ATP 1-1, the inorganic nanofibers are not able to form a connected network, hence most electrolyte actually is somewhat superficially absorbed, and cannot fully penetrate into the composite membrane to occupy the tiny pores, thus causing a low uptake.

Another wettability test backed the aforementioned conjecture by exhibiting the superior wettability of the SA/ATP membranes with electrolyte, where it is observed in Fig. 4b (top) that the immersion-height of all SA/ATP membranes is greater than that of the Celgard 2325 separator and SA/ATP 1-4 overwhelmingly wins out once again. More inspiringly, even after being placed in the fume hood for 2 h, the SA/ATP membranes still retained a considerable amount of electrolyte, while the Celgard 2325 had almost dried (Fig. 4b bottom). The results of BET analysis also offer more solid explanations towards this phenomenon. In Fig. S14, the SA/ATP membranes show IV-type adsorption and desorption isotherms, indicating their mesoporous feature. And indeed, as shown in the pore size distribution (Fig. 4c), these composite membranes possess much more pores with sizes less than 5 nm, which facilitate electrolyte absorption via strong capillary action. The combination of high surface area and nano-sized pores guarantees excellent electrolyte wettability and considerable electrolyte retention.

Better compatibility with liquid electrolyte then theoretically should engender higher ionic conductivity. As a critical factor to the performance of a cell, the ionic conductivity of SA/ATP membranes in electrolyte was measured by electrochemical impedance spectroscopy (EIS). As shown in Fig. 4d, it is found that the SA/ATP 1-4 has the highest conductivity in commercial liquid electrolyte among all membranes, even higher than that of Celgard 2325, which accords with the results of previous electrolyte wettability test. At room temperature, the ionic conductivity of SA/ATP 1-4 separator was measured to be 1.15 mS cm^{-1} , while that of Celgard 2325 separator was 0.95 mS cm^{-1} . A point worth noting is that, although other membranes containing less ATP also show better wettability with liquid electrolyte than their Celgard counterpart, their conductivity is inferior to that of the latter. It is also considered attributed to the "inactive" pores in SA and insufficient connection

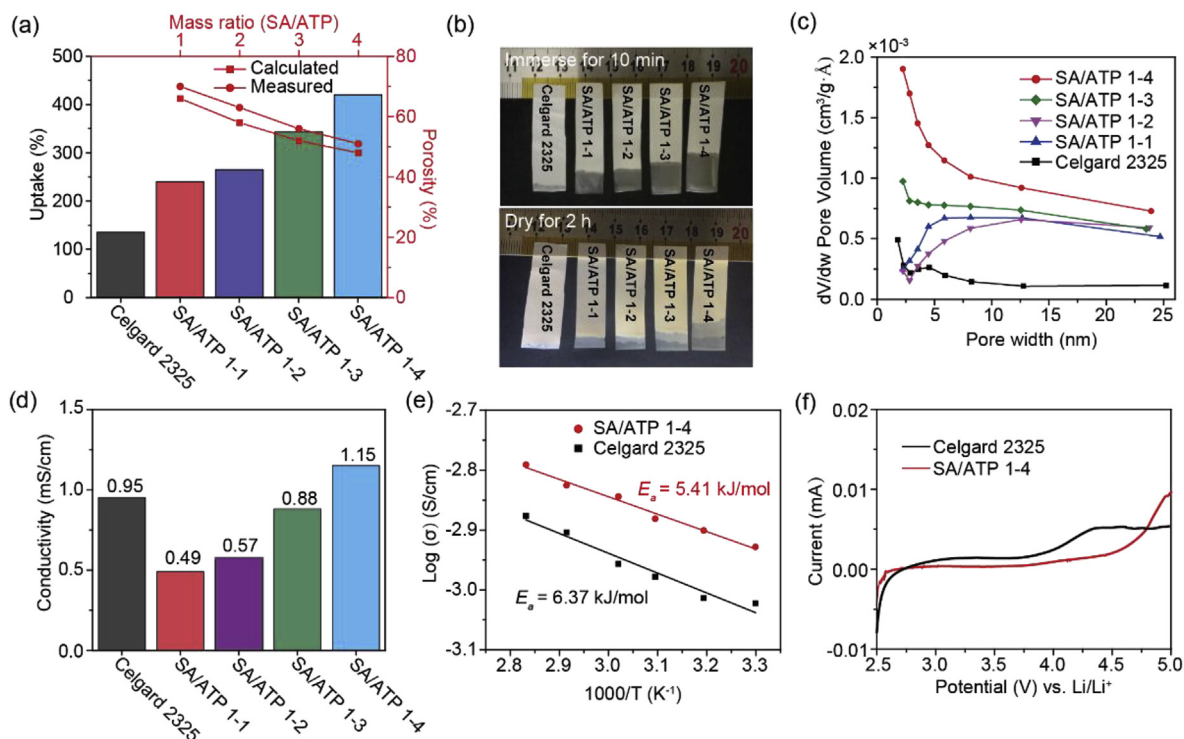


Fig. 4. The compatibility between Celgard 2325, SA/ATP separators and commercial carbonate electrolyte (1 M LiPF₆ in EC/DEC, (EC: DEC = 1:1, w/w)). (a) Electrolyte absorption capability and porosity of SA/ATP and Celgard separators. (b) Electrolyte immersion height of SA/ATP and Celgard separators after being immersed for 10 min (top) and after being placed in the fume hood for 2 h (bottom). (c) Pore size distribution of SA/ATP and Celgard 2325 separators. (d) Ionic conductivities of SA/ATP and Celgard 2325 separators in the commercial carbonate electrolyte at room temperature. (e) The Arrhenius plot of temperature-dependent ionic conductivity of Celgard 2325 and SA/ATP 1-4 separators. (f) Linear sweep voltammetry of Celgard 2325 and SA/ATP 1-4 separators.

among the ATP nanofibers, which prevents the liquid electrolyte from thoroughly permeating into the membrane and filling the tiny interior pores, hence leaving some amount of air bubbles inside and resulting in a low ionic conductivity.

The temperature-dependent ionic conductivity of the SA/ATP separator was plotted in Fig. 4e. It is inspiring to see that the activation energy of the SA/ATP 1-4 separator (5.41 kJ mol⁻¹ or 0.056 eV) is slightly lower than that of the Celgard 2325 separator (6.37 kJ mol⁻¹ or 0.066 eV), meaning that the lithium ions move more favorably in the SA/ATP 1-4 separator. As the SA/ATP 1-4 membrane possesses best wettability with liquid electrolyte and ionic conductivity among all membranes, it was chosen to assemble LiFePO₄ (LFP)/Li cells for the following rate capacity test and long cycling test.

But before that, LSV was first implemented to prove the electrochemical stability of SA/ATP 1-4 separator. As shown in Fig. 4f, the SA/ATP separator showed no evident reaction at voltage below 4.5 V. Therefore, the SA/ATP 1-4 separator is qualified to be used as the separator in lithium-ion batteries. Li/Li symmetric cells with Celgard 2325 or SA/ATP 1-4 separators at the current density of 1 mA cm⁻² were also cycled. As shown in Fig. S15a, the overpotential of the former started to increase dramatically after 200 h (615 mV in 280 h), while the latter only showed a slight increase in overpotential from 113 mV at the beginning to 148 mV after 350 h, proving that the SA/ATP separator leads to more stable lithium deposition and stripping. After cycling, the Li/Li symmetric cells were disassembled to observe the morphology of the lithium anode through SEM. It is shown that, compared with that in the cell using Celgard 2325 where lithium dendrites have evidently formed (Fig. S15b), the lithium metal in the cell using SA/ATP 1-4 exhibits a much smoother surface (Fig. S15c), meaning its nanopores realize a uniform flux of lithium ions during cycling and thereby suppressing the growth of dendrites.

The separator was further tested in LiFePO₄/Li cells. From the voltage-discharge capacity profiles in Fig. 5a, it is observed that the cell

using SA/ATP 1-4 membrane has a smaller overpotential and more stable charge/discharge plateaus in comparison to the cell using Celgard 2325, indicative of its excellent chemical stability and low resistance as the separator. Such SA/ATP separator also shows attractive power capability, as shown in Fig. 5b. The LFP/Li cell with SA/ATP 1-4 separator shows reversible specific capacity of 152, 145.5, 134.6, 128.9, 120.9 and 114.9 mAh g⁻¹ at C/2, 1 C, 2 C, 3 C, 4 C, and 5 C, respectively. Nevertheless, LFP/Li cell with Celgard separator shows specific capacity of 148.9, 143.1, 134.6, 126.5, 110.4 and 84.3 mAh g⁻¹ at C/2, 1 C, 2 C, 3 C, 4 C, and 5 C, respectively. When the rate was 3 C, the discharge capacity of both were quite stable. However, when it jumped to 4 C, the discharge capacity of the cell using Celgard 2325 started to descend dramatically. While in contrast, the discharge capacity of the cell using SA-ATP remained stable even until the rate reached 5 C. When the rate rebounded back to 1 C, the discharge capacity of both cells returned to the normal level, 144.9 mAh g⁻¹ and 142.4 mAh g⁻¹ for cells with SA/ATP 1-4 and Celgard 2325 separators, respectively.

The reliability of SA/ATP membranes in cells was also verified upon the long cycling test, where the cell using SA/ATP 1-4 membrane shows better performance than the cell using Celgard 2325 separator. From Fig. 5c, it is observed that after 500 cycles at 0.5C, the cell using SA/ATP separator gradually gained an advantage of higher capacity retention over that using Celgard 2325. When 700 cycles was approached, the discharge capacity of the former decreased from 150.2 mAh g⁻¹ to 123.5 mAh g⁻¹, with 82.2% capacity retention, while the discharge capacity of the latter decreases from 150 mAh g⁻¹ to 103.1 mAh g⁻¹, with only 68.7% capacity retention. Another long cycling test at the rate of 1 C was also conducted, which shows similar results (Fig. S16), where the cell using the SA/ATP 1-4 separator has higher discharge capacity and more capacity retention. The reason why SA/ATP 1-4 as the separator leads to a higher capacity retention is considered two-fold.

In the first place, the nano-porous structure with a considerably large surface area enables the composite membrane to retain more liquid

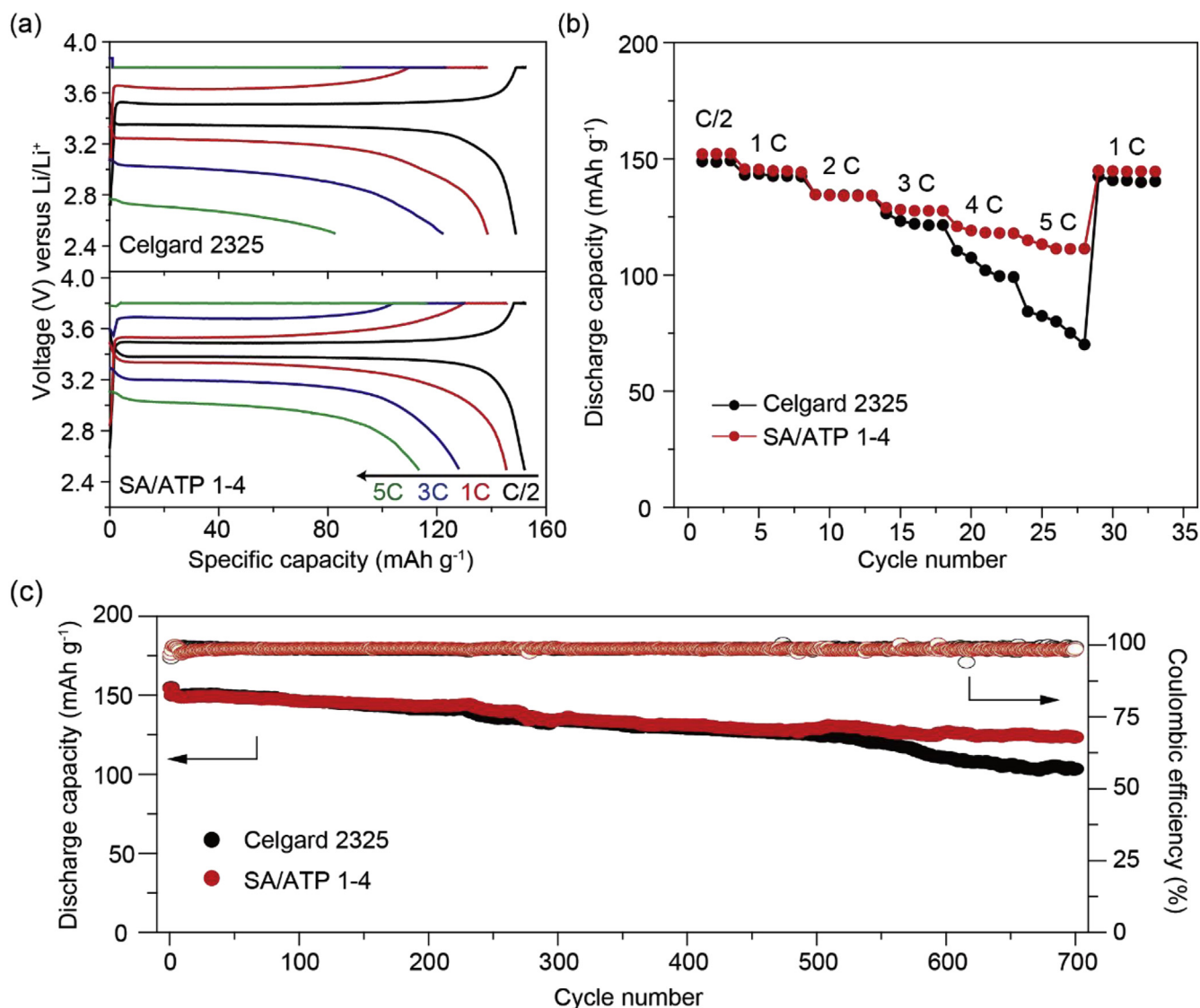


Fig. 5. Electrochemical performance of LFP/Li cells using Celgard 2325 and SA/ATP 1–4 membrane as the separators in the cut-off voltage range of 2.5–3.8 V. (a) Charge-discharge profiles of LFP/Li cells with Celgard and SA/ATP 1–4 separators at C/2, 1 C, 2 C, 3 C, 4 C and 5 C. (b) Rate performance of LFP/Li cells with Celgard and SA/ATP 1–4 separators at various C rates. (c) The long cycling performance of LFP/Li cells with Celgard 2325 and SA/ATP 1–4 separators at 0.5C. The mass loading of active material in cathode was fixed at 4.5 mg cm⁻² and 1 C was 170 mA g⁻¹.

electrolytes, which has been proved in previous test of electrolyte wettability. Secondly, most of its pores with sizes less than 10 nm realize more uniform current distribution during long cycling and constrain heterogeneity of the current within a significantly small scale, thereby improving the performance of lithium anode. While in sharp contrast, a typical Celgard separator features pore sizes around 100 nm. The dramatically ascending pore sizes then raise the possibility of the heterogeneity in current distribution across the interface between separator and electrodes, thus conceivably causing undesirable aftermath for the lithium anode. This assumption is backed by the morphology of the lithium anode after 700 cycles.

After cycling, the cells were disassembled to observe the change in morphology of lithium metal anode and separators via SEM. From Fig. 6a–c, the lithium anode of the cell using Celgard separator shows a much more porous and foam-like morphology, which causes the depletion of electrolyte and thereby accounts for the decay of its capacity. While in stark contrast, from Fig. 6e–g, it is shown that the nano-porous structure of the SA/ATP membrane remarkably contributes to the uniform deposition of lithium during cycling, enabling the formation of a compact surface of the lithium anode, which eventually gives birth to a

high capacity retention after long cycling. And besides retardancy to fire, the addition of ATP also brings some extra bonus. Through Fig. 6d, it is found that, after long cycling, the microstructure of Celgard separator has somewhat undergone deterioration, where some pores have closed compared to its original state (Fig. S5a) in which high porosity and uniform pore distribution are clearly observed. While in comparison, as shown in Fig. 6h, it is found that the ATP nanofibers are able to stretch the SA substrate and maintain the porous structure and the pore size to a great extent, preventing the membrane from swelling. Moreover, XRD was also conducted for the SA/ATP separator after cycling to offer some more insight. As shown in Fig. S17, there is no evident change in the pattern of the separator after 700 cycles, indicating its good electrochemical stability.

4. Conclusions

A composite membrane composed of sodium alginate as polymer substrate and attapulgite nanofiber as inorganic additive was synthesized through a phase inversion process, which has small pore sizes mainly ranging from a few to 25 nm. Compared with common Celgard 2325

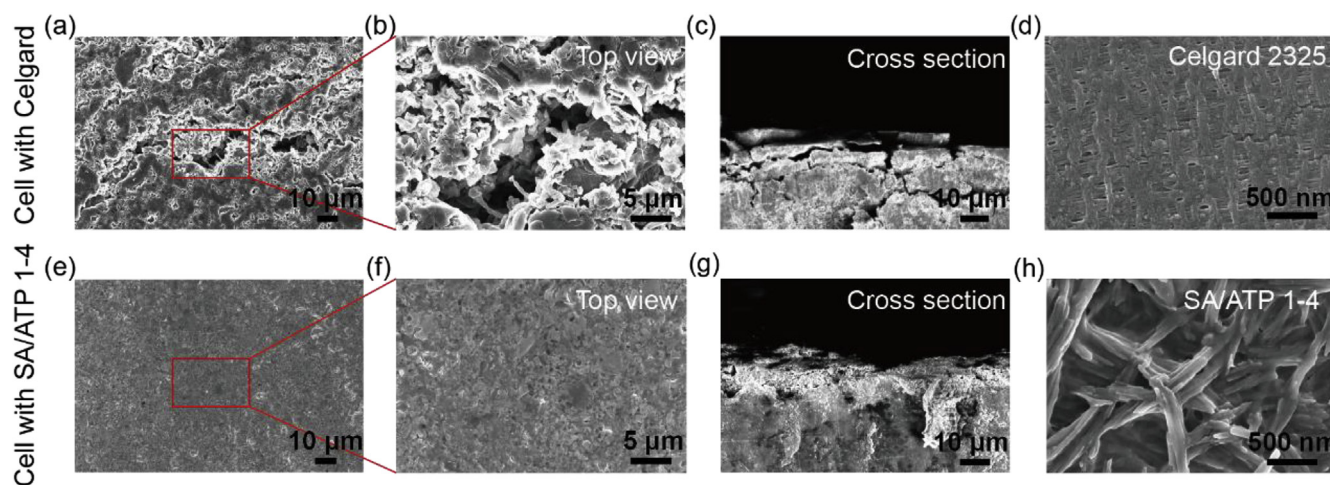


Fig. 6. SEM images of lithium anodes and separators derived from cycled LFP/Li cells. (a–b) Top view and (c) cross-section images of the lithium anode from cycled LFP/Li cell with Celgard 2325 separator. (d) SEM image of Celgard 2325 separator after 700 cycles. (e–f) Top view and (g) cross-section images of the lithium anode from cycled LFP/Li cell with SA/ATP 1–4 separator. (h) SEM image of SA/ATP 1–4 membrane after 700 cycles.

separator, the SA/ATP membrane with SA/ATP ratio of 1–4 is found to possess superior properties. The addition of ATP nanofibers endows the membrane with pronounced retardancy to fire and excellent thermal stability, that it does not catch on fire even wetted by liquid electrolyte and is able to maintain its dimension after being heated at 250 °C for 2 h while suffering almost no thermal shrinkage. By virtue of its super large specific surface, the SA/ATP 1–4 membrane has better wettability with liquid electrolyte as well, where its electrolyte uptake is 420%, more than three times as high as that of its Celgard counterpart. When used as the separator in LFP/Li cell, the SA/ATP 1–4 membrane exhibits higher conductivity and leads to high capacity retention of 82% after 700 cycles, and attractive rate capability of 115 mAh g⁻¹ at 5 C. The excellent electrochemical performance is ascribed to the nano-porous structure, which retains more electrolyte and enables uniform lithium deposition during cycling. Furthermore, as both ingredients are non-toxic and the sodium alginate is a commonly used biomaterial, this eco-friendly membrane can degrade in soil without causing any contamination. We believe this work sheds light on the possibility of utilizing biodegradable materials in real battery applications to help achieve a cleaner and greener future.

Acknowledgments

Y. Yang acknowledges support from Air Force Office of Scientific Research (FA9550-18-1-0410). The authors greatly appreciate the funding support from the NSF MRSEC program through Columbia in the Center for Precision Assembly of Superstratic and Superatomic Solids (DMR-1420634). A. J. Li would like to acknowledge the financial support from the China Scholarship Council (No. 201706010086) and X. Y. Chuan acknowledges the National Natural Science Foundation of China (No. 51774016).

Appendix A. Supplementary data

Supplementary data to this article can be found online at <https://doi.org/10.1016/j.ensm.2019.06.033>.

References

- D. Lin, Y. Liu, Y. Cui, Reviving the lithium metal anode for high-energy batteries, *Nat. Nanotechnol.* 12 (2017) 194.
- X.-B. Cheng, et al., Toward safe lithium metal anode in rechargeable batteries: a review, *Chem. Rev.* 117 (15) (2017) 10403–10473.
- A. Manthiram, X. Yu, S. Wang, Lithium battery chemistries enabled by solid-state electrolytes, *Nat. Rev. Mater.* 2 (2017) 16103.
- J. Liu, et al., Pathways for practical high-energy long-cycling lithium metal batteries, *Nat. Energy* 4 (3) (2019) 180–186. ISSN: 2058-7546.
- S.S. Zhang, A review on the separators of liquid electrolyte Li-ion batteries, *J. Power Sources* 164 (1) (2007) 351–364.
- M.-H. Ryou, et al., Mussel-inspired polydopamine-treated polyethylene separators for high-power Li-ion batteries, *Adv. Mater.* 23 (27) (2011) 3066–3070.
- J.-A. Choi, S.H. Kim, D.-W. Kim, Enhancement of thermal stability and cycling performance in lithium-ion cells through the use of ceramic-coated separators, *J. Power Sources* 195 (18) (2010) 6192–6196.
- H.-S. Jeong, S.-Y. Lee, Closely packed SiO₂ nanoparticles/poly(vinylidene fluoride-hexafluoropropylene) layers-coated polyethylene separators for lithium-ion batteries, *J. Power Sources* 196 (16) (2011) 6716–6722.
- N. Deng, et al., A review on separators for lithium-sulfur battery: progress and prospects, *J. Power Sources* 331 (2016) 132–155.
- X. Zeng, J. Li, N. Singh, Recycling of spent lithium-ion battery: a critical review, *Crit. Rev. Environ. Sci. Technol.* 44 (10) (2014) 1129–1165.
- G. Scott, D.M. Wiles, Programmed-life plastics from polyolefins: a new look at sustainability, *Biomacromolecules* 2 (3) (2001) 615–622.
- J. Zhang, et al., Sustainable, heat-resistant and flame-retardant cellulose-based composite separator for high-performance lithium ion battery, *Sci. Rep.* 4 (2014) 3935.
- H. Abdul Khalil, et al., Enhancement of basic properties of polysaccharide-based composites with organic and inorganic fillers: a review, *J. Appl. Polym. Sci.* 136 (12) (2019) 47251.
- K.Y. Lee, D.J. Mooney, Alginate: properties and biomedical applications, *Prog. Polym. Sci.* 37 (1) (2012) 106–126.
- J.S. Temenoff, A.G. Mikos, Tissue engineering for regeneration of articular cartilage, *Biomaterials* 21 (5) (2000) 431–440.
- K. Ishikawa, et al., Non-decay type fast-setting calcium phosphate cement: composite with sodium alginate, *Biomaterials* 16 (7) (1995) 527–532.
- L. Zhang, et al., Biomass-derived materials for electrochemical energy storages, *Prog. Polym. Sci.* 43 (2015) 136–164.
- I. Kovalenko, et al., A major constituent of brown algae for use in high-capacity Li-ion batteries, *Science* (2011) 1209150.
- J. Liu, et al., A high-performance alginate hydrogel binder for the Si/C anode of a Li-ion battery, *Chem. Commun.* 50 (48) (2014) 6386–6389.
- J. Li, et al., Enhanced performance of a MnO₂-graphene sheet cathode for lithium ion batteries using sodium alginate as a binder, *J. Mater. Chem.* 22 (26) (2012) 13002–13004.
- J. Liu, et al., A robust ion-conductive biopolymer as a binder for Si anodes of lithium-ion batteries, *Adv. Funct. Mater.* 25 (23) (2015) 3599–3605.
- H. Wen, et al., Sustainable and superior heat-resistant alginate nonwoven separator of LiNi_{0.5}Mn_{1.5}O₄/Li batteries operated at 55 °C, *ACS Appl. Mater. Interfaces* 9 (4) (2017) 3694–3701.
- J.-W. Jung, et al., Electrospun nanofibers as a platform for advanced secondary batteries: a comprehensive review, *J. Mater. Chem.* 4 (3) (2016) 703–750.
- P. Yao, et al., PVDF/Palygorskite nanowire composite electrolyte for 4 V rechargeable lithium batteries with high energy density, *Nano Lett.* 18 (10) (2018) 6113–6120.
- R.L. Frost, Z. Ding, Controlled rate thermal analysis and differential scanning calorimetry of sepiolites and palygorskites, *Thermochim. Acta* 397 (1–2) (2003) 119–128.
- S. Akyüz, T. Akyüz, J. Davies, An FT-IR spectroscopic investigation of the adsorption of benzidine by sepiolite from Eskisehir (Turkey), *J. Mol. Struct.* 293 (1993) 279–282.
- R. Schmich, et al., Performance and cost of materials for lithium-based rechargeable automotive batteries, *Nat. Energy* 3 (4) (2018) 267.
- J. Mandal, et al., Hierarchically porous polymer coatings for highly efficient passive daytime radiative cooling, *Science* 362 (6412) (2018) 315–319.

- [29] B. Xu, et al., Porous insulating matrix for lithium metal anode with long cycling stability and high power, *Energy Storage Mater.* 17 (2019) 31–37.
- [30] X. Huang, Separator technologies for lithium-ion batteries, *J. Solid State Electrochem.* 15 (4) (2011) 649–662.
- [31] H. Lee, et al., A review of recent developments in membrane separators for rechargeable lithium-ion batteries, *Energy Environ. Sci.* 7 (12) (2014) 3857–3886.
- [32] X. Hao, et al., Ultrastrong polyoxazole nanofiber membranes for dendrite-proof and heat-resistant battery separators, *Nano Lett.* 16 (5) (2016) 2981–2987.
- [33] P. Li, et al., Chitosan-alginate nanoparticles as a novel drug delivery system for nifedipine, *Int. J. Biomed. Sci.: IJBS* 4 (3) (2008) 221–228.
- [34] Z.L. He, G.K. Zhang, W. Xu, Enhanced adsorption of fluoride from aqueous solution using an iron-modified attapulgite adsorbent, *Water Environ. Res.* 85 (2) (2013) 167–174.
- [35] Q. Wang, et al., Thermal runaway caused fire and explosion of lithium ion battery, *J. Power Sources* 208 (2012) 210–224.
- [36] H.-Y. Li, et al., A thermally stable, combustion-resistant, and highly ion-conductive separator for lithium-ion batteries based on electrospun fiber mats of crosslinked polybenzoxazine, *Energy Technol.* 4 (4) (2016) 551–557.
- [37] S. Byun, et al., A crosslinked nonwoven separator based on an organosoluble polyimide for high-performance lithium-ion batteries, *J. Ind. Eng. Chem.* 72 (2019) 390–399.
- [38] J. Li, et al., Electrochemical performance and thermal stability of the electrospun PTFE nanofiber separator for lithium-ion batteries, *J. Appl. Polym. Sci.* 135 (29) (2018) 46508.